environments is unlikely for a hydrothermal system. There are no facies or thickness trends that indicate the existence of local sources of silica or other materials, such as hydrothermal vents, and no cross-cutting features or deposits that might represent syndepositional hydrothermal conduits or hot springs. Instead, silicification most probably resulted from precipitation out of a hot ocean[18] that had no biological sink for silica[9].

Mat-like laminations are restricted to shallow-water environments in an apparent ecological control of their distribution. Carbonaceous matter in the BRC has a carbon isotopic composition of −35 to −20‰ compared with PDB[14]. Although mechanisms have been proposed by which hydrothermal systems could produce isotopically fractionated methane[19], no hydrothermal systems capable of generating large volumes of fractionated carbonaceous matter consistently within this isotopic range are known.

The isotopic composition of BRC carbonaceous matter is consistent with fixation by autotrophs employing the Calvin cycle[20]. Organisms with a variety of physiologies use this pathway, including some types of oxygenic and anoxygenic photosynthesizers, and many chemoautotrophs such as sulphide, iron and hydrogen oxidizers[21]. The absence of ferric oxides in the platform facies implies that carbon was not fixed predominantly by iron oxidation. Sulphide and hydrogen oxidation both require free O_2. The presence of siderite and the absence of ferric oxides throughout the BRC indicates that the partial pressure of O_2 was very low, making both of these metabolisms unlikely as primary carbon-fixation pathways. During deposition of the BRC, mat-forming microorganisms were apparently confined to shallow-water settings above deep storm wave base. In modern oceans, this corresponds to depths of less than 200 m (ref. 22). Restriction of these communities to shallow water probably reflects confinement to the euphotic zone, which generally corresponds to depths of less than 150 m (ref. 23). Taken together, the carbon isotopic composition of BRC carbonaceous matter, the presence of siderite and lack of primary ferric oxides, and the restriction of microbial mats to shallow water indicate that photosynthetic, probably anoxygenic, microbes were active in the 3,416-Myr-old ocean.

Detrital carbonaceous grains become simpler in morphology and finer in size with the transition from shallow platform settings to deep platform and basin settings. This distribution is strongly indicative of a shallow-water origin for these grains, most probably ultimately by the erosion of shallow-water mats. Mat material was ripped up and redistributed as detritus in shallow marine environments by waves and storms. In deeper waters, fine detrital carbonaceous matter accumulated through hemipelagic settling along with precipitated siderite, fine clastic material, and silica. The BRC provides a clear window into ocean chemistry and structure and biological processes active about 3.4 Gyr ago. □

Received 9 January; accepted 26 July 2004; doi:10.1038/nature02888.

1. Schopf, J. W. & Packer, B. M. Early Archean (3.3 billion to 3.5 billion-year-old) microfossils from Warrawoona Group, Australia. *Science* **237,** 70–73 (1987).
2. Brasier, M. D. *et al.* Questioning the evidence for Earth's oldest fossils. *Nature* **416,** 76–81 (2002).
3. Garcia-Ruiz, J. M. *et al.* Self-assembled silica-carbonate structures and detection of ancient microfossils. *Science* **302,** 1194–1197 (2003).
4. Westall, F. *et al.* Early Archean fossil bacteria and biofilms in hydrothermally-influenced sediments from the Barberton greenstone belt, South Africa. *Precambr. Res.* **106,** 93–116 (2001).
5. Paris, I., Stanistreet, I. G. & Hughes, M. J. Cherts of the Barberton greenstone belt as products of submarine exhalative activity. *J. Geol.* **93,** 111–129 (1985).
6. Klein, C. & Beukes, N. J. Geochemistry and sedimentology of a facies transition from limstone to iron-formation deposition in the early Proterozoic Transvaal Supergroup, South Africa. *Econ. Geol.* **84,** 1733–1774 (1989).
7. Lowe, D. R. in *Early Life on Earth. Nobel Symposium No. 84* (ed. Bengston, S.) 24–35 (Columbia Univ. Press, New York, 1994).
8. Lowe, D. R. in *Geologic Evolution of the Barberton Greenstone Belt, South Africa* (eds Lowe, D. R. & Byerly, G. R.) 83–114 (Geol. Soc. Am. Spec. Pap. 329, Boulder, Colorado, 1999).
9. Siever, R. The silica cycle in the Precambrian. *Geochim. Cosmochim. Acta* **56,** 3265–3272 (1992).
10. Lowe, D. R. & Byerly, G. R. in *Geologic Evolution of the Barberton Greenstone Belt, South Africa* (eds Lowe, D. R. & Byerly, G. R.) 1–36 (Geol. Soc. Am. Spec. Pap. 329, Boulder, Colorado, 1999).
11. Lowe, D. R. & Fisher Worrell, G. in *Geologic Evolution of the Barberton Greenstone Belt, South Africa* (eds Lowe, D. R. & Byerly, G. R.) 167–188 (Geol. Soc. Am. Spec. Pap. 329, Boulder, Colorado, 1999).
12. Tice, M. M., Bostick, B. C. & Lowe, D. R. Thermal history of the 3.5–3.2 Ga Onverwacht and Fig Tree Groups, Barberton greenstone belt, South Africa. *Geology* **32,** 37–40 (2004).
13. Sumner, D. Y. Late Archean calcite–microbe interactions: Two morphologically distinct microbial communities that affected calcite nucleation differently. *Palaios* **12,** 302–318 (1997).
14. Walsh, M. M. & Lowe, D. R. in *Geologic Evolution of the Barberton Greenstone Belt, South Africa* (eds Lowe, D. R. & Byerly, G. R.) 115–132 (Geol. Soc. Am. Spec. Pap. 329, Boulder, Colorado, 1999).
15. Simonson, B. M., Schubel, K. A. & Hassler, S. W. Carbonate sedimentology of the early Precambrian Hamersley Group of Western Australia. *Precambr. Res.* **60,** 287–335 (1993).
16. Lowe, D. R. & Byerly, G. R. Ironstone pods in the Archean Barberton greenstone belt, South Africa: Earth's oldest seafloor hydrothermal vents reinterpreted as Quaternary subaerial springs. *Geology* **31,** 909–912 (2003).
17. de Wit, M. J., Hart, R., Martin, A. & Abbott, P. Archean abiogenic and probable biogenic structures associated with mineralized hydrothermal vent systems and regional metasomatism, with implications for greenstone belt studies. *Econ. Geol.* **77,** 1783–1802 (1982).
18. Knauth, L. P. & Lowe, D. R. High Archean climatic temperature inferred from oxygen isotope geochemistry of cherts in the 3.5 Ga Swaziland Supergroup, South Africa. *Geol. Soc. Am. Bull.* **115,** 566–580 (2003).
19. Horita, J. & Berndt, M. E. Abiogenic methane formation and isotopic fractionation under hydrothermal conditions. *Science* **285,** 1055–1057 (1999).
20. Schidlowski, M. in *Microbial Sediments* (eds Riding, R. E. & Awramik, S. M.) 84–95 (Springer, New York, 2000).
21. Madigan, M. T., Martinko, J. M. & Parker, J. *Brock Biology of Microorganisms* (Prentice-Hall, Upper Saddle River, New Jersey, 1997).
22. Boggs, S. *Principles of Sedimentology and Stratigraphy* (Prentice-Hall, Englewood Cliffs, New Jersey, 1995).
23. Lalli, C. M. & Parsons, T. R. *Biological Oceanography: An Introduction* (Butterworth-Heinemann, Boston, 1997).

Acknowledgements This work was supported by NASA Exobiology Program grants to D.L. M.T. was also supported by a William R. and Sara Hart Kimball Stanford Graduate Fellowship and by a Harvey Fellowship.

Competing interests statement The authors declare that they have no competing financial interests.

Correspondence and requests for materials should be addressed to M.T. (mtice@pangea.stanford.edu).

Excitation of Earth's continuous free oscillations by atmosphere–ocean–seafloor coupling

Junkee Rhie & Barbara Romanowicz

Berkeley Seismological Laboratory and Department of Earth and Planetary Science, University of California, Berkeley, California 94720, USA

The Earth undergoes continuous oscillations, and free oscillation peaks have been consistently identified in seismic records in the frequency range 2–7 mHz (refs 1, 2), on days without significant earthquakes. The level of daily excitation of this 'hum' is equivalent to that of magnitude 5.75 to 6.0 earthquakes[3,4], which cannot be explained by summing the contributions of small earthquakes[1,3]. As slow or silent earthquakes have been ruled out as a source for the hum[4] (except in a few isolated cases[5]), turbulent motions in the atmosphere or processes in the oceans have been invoked[3,6–8] as the excitation mechanism. We have developed an array-based method to detect and locate sources of the excitation of the hum. Our results demonstrate that the Earth's hum originates mainly in the northern Pacific Ocean during Northern Hemisphere winter, and in the Southern oceans during Southern Hemisphere winter. We conclude that the Earth's hum is generated by the interaction between atmosphere, ocean and sea floor, probably through the conversion of storm energy to oceanic infragravity waves that interact with seafloor topography.

Elucidating the physical mechanism responsible for the continuous oscillations represents an intriguing scientific challenge. The source(s) should be close to the Earth's surface, as the fundamental

mode appears to be preferentially excited. One proposed mechanism relates the observed oscillations to random excitation by turbulent motions in the atmosphere[3,6,7]. Amplitude levels and frequency dependence estimated stochastically, and constrained by actual barometer readings, are in agreement with the observed continuous oscillation levels. Also in support of this interpretation, seasonal variations in the level of energy present in the continuous oscillations have a six-month periodicity, with maxima in January and July corresponding to winter in Northern and Southern hemispheres respectively[4], correlated with maxima in average atmospheric pressure variations. On the other hand, Nishida and Kobayashi[9] proposed that the source might be distributed over the entire surface of the Earth. The fact that the background mode signal can be brought out even more clearly by correcting the observed spectra for signal correlated with local barograph recordings provides further evidence for the non-local character of the excitation process[10]. An alternative potential source of excitation of the 'hum' could be in the oceans, resulting from interaction between wind and ocean waves. Such an interpretation is supported by the similarity of the shape of ocean-bottom pressure spectra and ground-motion noise spectra[8].

In order to make further progress on this issue, it is important to determine whether the excitation source is indeed distributed over most of the Earth, or whether most of it occurs either in the oceans or on land. The approaches used so far, based on the computation of spectra, or the correlation of signals across full great-circle paths[4], allow the detection but not the location of the sources. The latter must be addressed using a propagating wave methodology.

We have developed an array-based method to detect and locate sources of very-long-period surface wave energy, using the dispersive properties of Rayleigh waves[11]. The use of surface waves to detect and locate earthquakes was proposed many decades ago[12]. Generally, moderate size events and relatively short periods (that is, 20–100 s) have been considered[13]. Array methods have been developed and applied widely for detection and analysis of body waves in the azimuth-slowness domain[14], and for the analysis of sources of microseisms[15,16]. Recently, Ekström *et al.*[17] developed a stacking technique based on a global network of ~100 long-period seismic stations and, in the period band 35–150 s, they detected many glacial earthquakes depleted in high-frequency energy. On the other hand, Nishida *et al.*[18] showed that the vertical seismic background noise in the entire pass-band from 2 to 20 mHz is dominated by globally propagating Rayleigh waves. Here we utilize the dispersive properties of mantle Rayleigh waves in the period band 150–500 s across two regional networks of very broadband seismometers, one in Japan (F-net) and the other in California (BDSN). Our analysis is centred around a period of 240 s, where the dispersion of Rayleigh waves presents a characteristic Airy phase. For each array, time domain seismograms are stacked after correcting for dispersion and attenuation across the array, assuming plane wave propagation from an arbitrary azimuth (see Methods, and Supplementary Fig. 1). We first exercised and tested the array sensitivity on real earthquake data, for the two-year period 2000–01.

In order to attempt detection and location of non-earthquake sources of surface wave energy, it is necessary to first remove all intervals of time affected by earthquakes of moment magnitude $M_w > 5.5$ (see Methods), whereas smaller earthquakes do not significantly contribute to Rayleigh wave energy above 150 s (refs 1, 2). Many detections of Rayleigh wave energy are observed

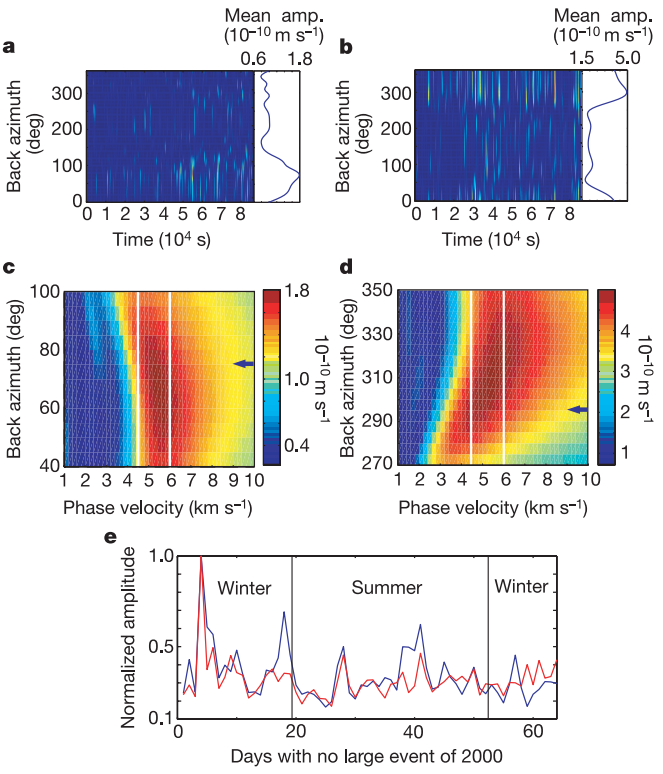

Figure 1 Analysis of detections for 31 January 2000. **a**, Amplitude of F-net stacks as a function of time and back azimuth. Small panel on right shows mean amplitude, as a function of back azimuth. A gaussian filter centred at 240 s has been applied to waveforms before stacking. **b**, Same as **a** for BDSN. **c**, Mean amplitude plot as a function of phase velocity and back azimuth for F-net, confirming that the observed energy corresponds to Rayleigh wave arrivals. The two vertical white lines indicate the range of phase velocities expected for Rayleigh waves between periods of 200 and 400 s. The theoretical phase velocity at 240 s is 4.85 km s^{-1}. Blue arrow indicates the back azimuth of the maximum mean amplitude shown in **a**. **d**, Same as **c** for BDSN. **e**, Mean amplitude of stacks as a function of time for quiet days for BDSN (red) and F-net (blue), for back azimuths of 295° and 65° respectively, in winter and back azimuths 105° and 235° in summer, normalized to the maximum amplitude for the entire time span. These azimuths correspond to the average direction of maximum amplitude in each season. The correlation coefficient between the two time series is 0.78.

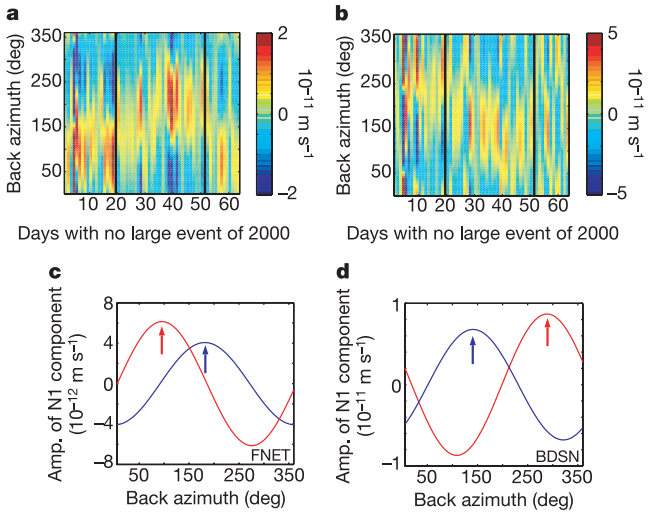

Figure 2 Amplitude of degree one as a function of time and back azimuth for the 64 quiet days in 2000. A 'quiet day' contains at least 12 contiguous hours uncontaminated by earthquakes, and only those intervals are considered within each day. **a**, Back azimuth corresponding to the maximum in the degree one component of stack amplitude for F-net as a function of time. Black vertical lines separate winter and summer intervals. Winter is defined as January–March, and October–December. **b**, Same as **a** for BDSN. **c**, Degree one as a function of azimuth for F-net, averaged for the winter (red) and the summer (blue). Arrows point to maxima in back azimuth; the degree one is almost as large as degree two in the data (see, for example, Supplementary Fig. 5) and is not contaminated by array response. **d**, Same as **c** for BDSN.

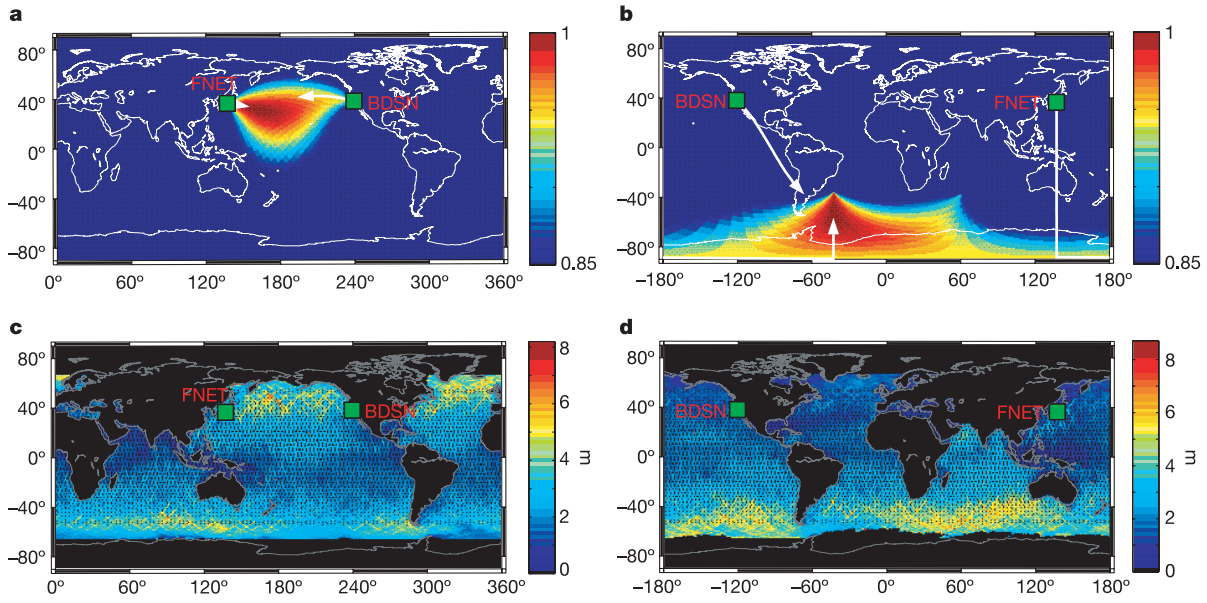

Figure 3 Comparison of seasonal variations in the distribution of hum-related noise (degree one only) and significant wave height in the year 2000. **a**, **b**, The directions corresponding to mean amplitudes that are larger than 85% of the maximum are combined for the two arrays in winter (**a**) and in summer (**b**) to obtain the region of predominant sources in each season. Arrows indicate the direction of maxima. Both arrays are pointing to the North Pacific Ocean in the winter and to the southern oceans in the summer. **c**, **d**, Global distribution of significant wave height, in the winter (**c**) and in the summer (**d**), averaged from TOPEX/Poseidon images for the months of January and July 2000, respectively. Black colour in **c** and **d** indicates locations with no data.

on quiet days, unrelated to earthquakes (see, for example, Fig. 1a–d). Maximum stack amplitudes for BDSN and F-net correlate strongly as a function of time, indicating that the source of the Rayleigh wave 'noise' is common for the two arrays (Fig. 1e). Moreover, inspection of the Rayleigh wave energy distribution as a function of time and direction of arrival reveals striking spatial coherency. Because the array shape can introduce artificial distortions in the amplitude patterns as a function of azimuth, we first consider a component of the energy which is independent of the array response. For each day and for each array, we compute the Fourier spectrum of the stack amplitude as a function of azimuth and compare it to that of the array response (See Methods and Supplementary Information). The distribution of stack amplitudes as a function of time and back azimuth has a strong 'degree one' harmonic component in azimuth. This cannot be due to the array response which is dominated by even harmonics in azimuth, and indicates a true preferential direction of arrival. For each array, the direction of the maximum in degree one is stable at the seasonal scale; it is consistently different in (Northern Hemisphere) winter and summer (Fig. 2a, b). Then for each array, we compute the amplitude of the stack as a function of azimuth, averaged over summer and winter separately, calculate its Fourier spectrum and extract the degree one component (Fig. 2c, d) as well as the azimuth of the corresponding maximum. By combining the directions of maximum stack amplitude obtained for each array, in summer and winter respectively, and back-projecting along the corresponding great-circle paths, we infer that the sources locate preferentially in the northern Pacific Ocean in the winter (Fig. 3a), and in the southern oceans in the summer (Fig. 3b). These locations correspond to regions of maximum storm activity in the northern and southern winters respectively, as indicated by the comparison with significant wave height maps (Fig. 3c, d).

The degree one distribution only gives a first-order idea of the preferential direction of arrival at each array. More insight is obtained by determining how a distribution of sources, initially uniform in azimuth, needs to be modified to fit the original observed seasonal patterns. Such an analysis (See Methods, and Supplementary Figs 6 and 7) confirms that, in the winter, much of the energy originates in the North Pacific Ocean, while in the summer, the activity shifts to the southern seas. We have also verified (through forward modelling experiments described in detail in Supplementary Information) that distributions of sources over continental areas are not compatible with the observations at both arrays simultaneously, whereas even a rough preferential distribution of sources in the northern Pacific fits the winter patterns for both arrays rather well. In the summer, we require a distribution of sources in the southern oceans, with preferential contributions from parts of the south Pacific and south Atlantic. Although a precise location of the sources would necessitate a more precise knowledge of the array response, our experiments clearly show that neither a uniform distribution of sources around the globe nor a distribution over continents are compatible with the data, in contrast to a distribution alternating between northern and southern oceans in winter and summer, respectively.

Finally, we considered a particular day, 31 January 2000, which corresponds to a maximum in the amplitude of the stacks for both F-Net and BDSN (Fig. 1e). We computed the stack amplitude as a function of azimuth over this 24 h interval at each array (Fig. 1a, b), and noted that the maximum average stack amplitude over this time interval points to a well defined direction of arrival, which is in general agreement with that found on other winter days. We confirm that the energy maxima correspond to the arrival of Rayleigh waves (Fig. 1c, d) by searching for the phase velocity and azimuth which give the maximum stack amplitude, averaged over that day. To analyse the time/space distribution of these sources, we conducted a parameter search in and around the north Pacific region. We find that the sources are distributed in space and time over a region spanning several thousand km^2, and with a correlation time of the order of ~6 h (Fig. 4).

Our results show that the ocean plays a key role in the excitation of the Earth's 'hum'. Part of the energy contained in ocean waves (generated by significant storms over the mid-latitude oceans) is converted to elastic waves. Infragravity waves are obvious candidates for the energy transfer from storms, through the ocean, to the sea floor[19]. They are indirectly driven by winds over ocean basins, and are probably generated in shallow water through conversion from short-period ocean waves by nonlinear processes[20]. Some of

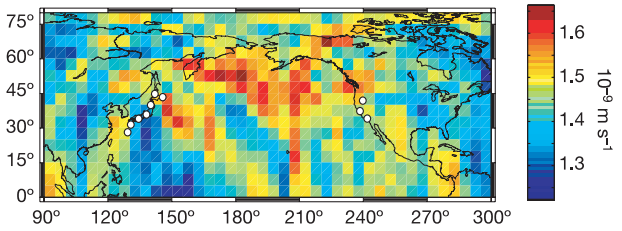

Figure 4 Distribution of sources for a 6 h time window on 31 January 2000 (from 14:00 to 20:00 UTC). Maximum amplitudes were averaged over all stations considered (in m s^{-1}), back-projected to the centre of 5° × 5° blocks, and corrected for the dispersion of Rayleigh waves for each source station path, thereby indicating the distribution of possible source locations. F-net, BDSN (with 3 TERRAscope stations) and 10 European stations (KONO, ARU, BFO, DPC, KIEV, SSB, AQU, VSL, ESK and ISP) are used in this analysis. White dots in Japan and California indicate the areas spanned by the corresponding arrays. Waveforms have been band-pass filtered between 150 and 500 s. Analysis over shorter time windows does not lead to stable results, suggesting a correlation time of several hours and a spatially distributed source. In this analysis, the plane wave approximation is not made, nor are the results biased by the array response.

the energy leaks out and propagates as free waves into the ocean basins[21]. Hydrodynamic filtering may play a role in determining where the coupling occurs, in that it limits the frequency band in which infragravity waves interact with the deep ocean floor[22], with shorter-period waves generated nearer to the coasts. The mechanism of generation of elastic waves probably involves focusing of infragravity waves by the concave shape of the continental boundaries towards the deep ocean, as well as by topography of the deep ocean floor. The efficiency with which long-period Rayleigh waves are generated in particular areas of the ocean basins must thus depend on the depth of the ocean floor, the shape of the continental shelves bounding the ocean basin, as well as the strength and persistence of storms. Notably, even though individual storms can be as strong over the north Atlantic as they are over the north Pacific, only the latter is detected in our data, which is in agreement with differences of 20-30 dB in pressure noise between these oceans in the infragravity wave band[23].

More detailed understanding of source distribution in space and time and its relation to ocean storms will require expanding the observational time windows by precisely removing signals due to earthquakes through a forward modelling approach, as is feasible at present with the availability of good quality three-dimensional elastic models of the mantle[24] as well as further analysis of wave height information. Also, the deployment of high-quality very broadband seismometers in the Southern Hemisphere (for example, across Australia) would help to characterize the source distribution better. Finally, we note that multi-disciplinary long-term ocean observatories spanning the entire water column (from sea floor to sea surface), such as are being proposed in the framework of the OOI (Ocean Observatories Initiative) programme[25], should acquire data that would help to make progress in our understanding of this complex energy transfer process. □

Methods

Array detection and location

We consider two regional networks of very broadband seismic stations in the Northern Hemisphere: (1) the Berkeley Digital Seismic Network (BDSN) in northern California, augmented by several stations of the TERRAscope network in southern California; and (2) the F-net in Japan. BDSN and F-net stations are equipped with very broadband STS-1 seismometers[26].

We pre-process vertical component time series by removing glitches and tides and deconvolving the instrument response to velocity. We then filter the data using either a gaussian filter centred at 240 s, or, in some experiments, a band-pass filter between 150 and 500 s (Fig. 4, Supplementary Fig. 4g). Two approximations are considered. We ignore the effect of lateral heterogeneity on the propagation of mantle Rayleigh waves, and we assume that they propagate across an array as plane waves (Supplementary Fig. 1), with a well defined incident azimuth (except in Fig. 4, where the plane wave approximation is not used). The whole year is divided into 1-day intervals. For each time interval, and for each increment in back azimuth of 5°, we align the waveforms from 10 or more stations using the centre of the array as reference point, and correct for dispersion and attenuation of the fundamental mode Rayleigh wave across the array, according to the reference PREM velocity model[27]. We stack the corrected waveforms using a phase weighted stack[28], which reduces uncorrelated noise, as compared to straight stacking (Supplementary Fig. 2). We tested the sensitivity of our array stacking for the detection of known earthquakes (Supplementary Information, Supplementary Figs 2, 3). Associating the detections obtained at three different arrays (including an array in western Europe) leads to an earthquake location method, not further described here, which works well at the magnitude 6 level, as we were able to detect and locate 85% of magnitude 6 and larger earthquakes without any optimization of the method.

Removal of intervals of time contaminated by earthquakes

We removed intervals of time of variable length, according to the size of the earthquake, for all earthquakes of magnitude $M_w > 5.5$. We first rejected any day within which an earthquake of $M_w > 6$ has occurred. We then defined a time span for additional rejection, using an exponential function constrained to be 3 days for $M_w \geq 7$, and 1.5 days for $M_w \geq 6$, starting at the origin time of the event. We also rejected a window before the earthquake, of length 10% of the length rejected following the origin time, to account for contamination due to the non-causal low-frequency filtering of the data. There are only a few 'quiet' windows left in one year, corresponding to ~18% of the time in 2000. Similar results are obtained for 2001.

Detection of Rayleigh waves during 'quiet' intervals

The same approach as used for detecting earthquakes is applied during quiet intervals. Supplementary Fig. 4 shows an example for a specific interval of time during day 2000/01/31, the same day as shown in Fig. 1. Alignment of traces is improved after taking into account Rayleigh wave dispersion in a specific azimuth range (Supplementary Fig. 4b, c). The corresponding stack amplitude has a maximum which is localized in time and azimuth (Supplementary Fig. 4a). The detected energy indeed corresponds to Rayleigh waves, as verified by a parameter search in azimuth and phase velocity space (Supplementary Fig. 4f) as well as in period versus phase velocity space (Supplementary Fig. 4g).

Removal of array response

Because the arrays considered are not completely symmetric, it is important to verify that biases due to the non-uniform array response in azimuth are not dominating the results. For this purpose, we have estimated the array response by randomly generating many synthetic seismograms and distributing them uniformly in azimuth. This procedure is described in detail in Supplementary Methods.

The amplitude of the array response cannot be directly compared to that of the observed patterns, so that we cannot completely remove it from the observed stack amplitudes. However, the array response has almost perfect 180° symmetry, with amplitude lobes corresponding to the elongated direction of the array, as expected. The corresponding Fourier spectra in azimuth are dominated by even degrees (particularly degree two), and have practically no degree one. In contrast, the spectra of the observed amplitude variations have a significant degree one (of a similar size as degree two, Supplementary Fig. 5e, f), which defines a specific direction of maximum amplitude, different in the summer from in the winter (Fig. 2). By conservatively analysing only the degree one component in the data, we guarantee that there is no contamination by the array response, while losing some directional resolution contained in the higher-degree azimuthal terms. Further experiments, as described in the main text and in Supplementary Information, confirm that the degree one analysis indeed gives a good indication of the spatial distribution of source energy and its seasonal variations.

Received 21 January; accepted 11 August 2004; doi:10.1038/nature02942.

1. Suda, N., Nawa, K. & Fukao, Y. Earth's background free oscillations. *Science* **279,** 2089–2091 (1998).
2. Tanimoto, T., Um, J., Nishida, K. & Kobayashi, N. Earth's continuous oscillations observed on seismically quiet days. *Geophys. Res. Lett.* **25,** 1553–1556 (1998).
3. Tanimoto, T. & Um, J. Cause of continuous oscillations of the Earth. *J. Geophys. Res.* **104,** 28723–28739 (1999).
4. Ekström, G. Time domain analysis of Earth's long-period background seismic radiation. *J. Geophys. Res.* **106,** 26483–26493 (2001).
5. Beroza, G. & Jordan, T. H. Searching for slow and silent earthquakes using free oscillations. *J. Geophys. Res.* **95,** 2485–2510 (1990).
6. Kobayashi, N. & Nishida, N. Continuous excitation of planetary free oscillations by atmospheric disturbances. *Nature* **395,** 357–360 (1998).
7. Fukao, Y., Nishida, K., Suda, N., Nawa, K. & Kobayashi, N. A theory of the Earth's background free oscillations. *J. Geophys. Res.* **107,** doi:10.1029/2001JB000153 (2002).
8. Watada, S. & Masters, G. Oceanic excitation of the continuous oscillations of the Earth. *Eos* **82,** F871 (2001).
9. Nishida, K. & Kobayashi, N. Statistical features of Earth's continuous free oscillations. *J. Geophys. Res.* **104,** 28741–28750 (1999).
10. Roult, G. & Crawford, W. Analysis of 'background' free oscillations and how to improve resolution by subtracting the atmospheric pressure signal. *Phys. Earth Planet. Inter.* **121,** 325–338 (2000).
11. Rhie, J. & Romanowicz, B. Detection and location of potential sources of background low frequency surface wave energy. *Eos* **83** (Fall Meet. Suppl.), abstr. S12A–1184 (2002).
12. von Seggern, D. Relative location of seismic events using surface waves. *Geophys. J.R. Astron. Soc.* **26,** 499–513 (1972).
13. Rouland, D., Condis, C., Parmentier, C. & Souriau, A. Previously undetected earthquakes in the Southern Hemisphere from long-period Geoscope data. *Bull. Seismol. Soc. Am.* **82,** 2448–2463 (1992).

14. Rost, S. & Thomas, C. Array seismology: Method and applications. *Rev. Geophys.* **40,** doi:10.1029/2000RG000100 (2002).
15. Friedrich, A., Kruger, F. & Klinge, K. Ocean-generated microseismic noise located with the GRFO array. *J. Seismol.* **2,** 47–64 (1998).
16. Schulte-Pelkum, V., Earle, P. S. & Vernon, F. L. Strong directivity of ocean-generated seismic noise. *Geochem. Geophys. Geosyst.* **5,** doi:10.1029/2003GC000520 (2004).
17. Ekström, G., Nettles, M. & Abers, G. A. Glacial earthquakes. *Science* **302,** 622–624 (2003).
18. Nishida, K., Kobayashi, N. & Fukao, Y. Origin of Earth's ground noise from 2 to 20 mHz. *Geophys. Res. Lett.* **29,** doi:10.1029/2001GL013862 (2002).
19. Tanimoto, T. Jet stream, roaming ocean waves, and ringing Earth. *Eos* **84** (Fall Meet. Suppl.), abstr. S12F–04 (2003).
20. Webb, S., Zhang, X. & Crawford, W. Infragravity waves in the deep ocean. *J. Geophys. Res.* **96,** 2723–2736 (1991).
21. Munk, W., Snodgrass, F. & Gilbert, F. Long waves on the continental shelf: an experiment to separate trapped and leaking modes. *J. Fluid Mech.* **20,** 529–554 (1964).
22. Webb, S. & Crawford, W. Long-period seafloor seismology and deformation under ocean waves. *Bull. Seismol. Soc. Am.* **89,** 1535–1542 (1999).
23. Webb, S. Broadband seismology and noise under the ocean. *Rev. Geophys.* **36,** 105–142 (1995).
24. Ekström, G., Tromp, J. & Larson, E. Measurements and models of global surface wave propagation. *J. Geophys. Res.* **102,** 8137–8157 (1997).
25. Committee for Implementation of a Seafloor Observatory Network for Oceanographic Research. *Enabling Ocean Research in the 21st Century: Implementation of a Network of Ocean Observatories* (Ocean Studies Board, National Academies Press, Washington DC, 2003).
26. Wielandt, E. & Streckeisen, G. The leaf spring seismometer: design and performance. *Bull. Seismol. Soc. Am.* **72,** 2349–2367 (1982).
27. Dziewonski, A. M. & Anderson, D. L. Preliminary reference Earth model. *Phys. Earth Planet. Inter.* **25,** 297–356 (1981).
28. Schimmel, M. & Paulssen, H. Noise detection and reduction of weak, coherent signals through phase-weighted stacks. *Geophys. J. Int.* **130,** 497–505 (1997).

Supplementary Information accompanies the paper on **www.nature.com/nature**.

Acknowledgements We thank the operators of the following seismic networks for making their data publicly available: BDSN (http://www.seismo.berkeley.edu), F-net (http://www.fnet.bosai.go.jp/freesia/index.html), IRIS (http://www.iris.edu) and TERRAscope. The Monthly Mean Global Surface Ocean Variables were obtained from the Physical Oceanography Distributed Active Archive Center (http://podaac.jpl.nasa.gov/poet). This work was partially supported by the NSF.

Competing interests statement The authors declare that they have no competing financial interests.

Correspondence and requests for materials should be addressed to B.R. (barbara@seismo.berkeley.edu).

Two new carnivores from an unusual late Tertiary forest biota in eastern North America

Steven C. Wallace[1] **& Xiaoming Wang**[2]

[1]*Department of Physics, Astronomy, and Geology, East Tennessee State University, Box 70636, Johnson City, Tennessee 37614, USA*
[2]*Department of Vertebrate Paleontology, Natural History Museum of Los Angeles County, 900 Exposition Boulevard, Los Angeles, California 90007, USA*

Late Cenozoic terrestrial fossil records of North America are biased by a predominance of mid-latitude deposits, mostly in the western half of the continent. Consequently, the biological history of eastern North America, including the eastern deciduous forest, remains largely hidden. Unfortunately, vertebrate fossil sites from this vast region are rare[1,2], and few pertain to the critically important late Tertiary period, during which intensified global climatic changes took place[3,4]. Moreover, strong phylogenetic affinities between the flora of eastern North America and eastern Asia clearly demonstrate formerly contiguous connections, but disparity among shared genera (eastern Asia–eastern North America disjunction) implies significant periods of separation since at least the Miocene epoch[1,2]. Lacustrine sediments deposited within a former sinkhole in the southern Appalachian Mountains provide a rare example of a late Miocene to early Pliocene terrestrial biota from a forested ecosystem[5]. Here we show that the vertebrate remains contained within this deposit represent a unique combination of North American and Eurasian taxa. A new genus and species of the red (lesser) panda (*Pristinailurus bristoli*), the earliest and most primitive so far known, was recovered. Also among the fauna are a new species of Eurasian badger (*Arctomeles dimolodontus*) and the largest concentration of fossil tapirs ever recorded. Cladistical analyses of the two new carnivores strongly suggest immigration events that were earlier than and distinct from previous records[6,7], and that the close faunal affinities between eastern North America and eastern Asia in the late Tertiary period are consistent with the contemporaneous botanical record[8,9].

The Gray Fossil Site consists of a sequence of finely laminated clays, silts and fine sands intermixed with isolated gravel lenses that fill a former sinkhole within the Cambrian/Ordovician Knox Group near the small community of Gray in Washington Co., Tennessee. The deposit covers roughly 1.8–2.0 ha, is up to 39 m thick and is the result of a small lake or pond that formed within the sinkhole. Subsequent weathering and erosion of the enclosing bedrock has generated a reversed topography, leaving the site as a high point on the landscape.

Vertebrate taxa such as *Tapiravus*, *Plionarctos*, *Pristinailurus* and *Arctomeles* (Table 1, left column) and abundant plant macrofossils (Table 1, right column) from *Quercus* (acorns) and *Carya* (hickory nuts) indicate that a dense forest surrounded the former 'pond'. *Quercus* and *Carya* constitute nearly 70% of initial pollen samples, and except for *Pinus* (which accounts for roughly 9% of the pollen count), the remaining taxa seem to be minor components of the flora. Both micro- and macrofossils reveal an arboreal flora, which was similar to that found in lower elevations of the southern Appalachians today.

The stratigraphic range of the rhino *Teleoceras*[10,11] and the short-faced bear *Plionarctos*[12,13] constrain the age of the assemblage to between 4.5 and 7 Myr (late Miocene to early Pliocene). This age is important because it occurs subsequent to the C_3/C_4 plant transition[4]; that is, when grasses first become dominant in many ecosystems worldwide[14], leading to the prevalence of many grassland-adapted taxa (horses, camels, antilocaprids and so on) within other Miocene/Pliocene faunas (particularly in North America). However, the absence of these grassland-adapted taxa and the predominance of forest-adapted taxa (Table 1) suggest that the Gray Fossil Site may have acted as a refugium from the changing

Table 1 **Vertebrate* and pollen taxa from the Gray Fossil Site**

Vertebrates	Pollens
Reptilia	Conifers
Trachemys sp.[20]	*Pinus* (pine)
Chrysemys sp.	*Tsuga* (hemlock)
Alligator sp.	Deciduous
cf. *Sistrurus* sp.[20]	*Quercus* (oak)
cf. *Regina* sp.[20]	*Carya* (hickory)
Aves	*Ulmus* (elm)
Passeriformes	*Betula* (birch)
Mammalia	*Fraxinus* (ash)
Soricidae	*Celtis* (hackberry)
Rodentia	Shrubs
Gomphotheridae	*Alnus* (alder)
Tapiravus polkensis	*Salix* (willow)
Teleoceras sp.	Herbs
Tayassuidae	*Ambrosia*-type ('ragweed')
cf. *Megatylopus* sp.	Cyperaceae (sedge)
cf. *Machairodus* sp.	Gramineae (grass)
Plionarctos sp.	Umbelliferae (parsely family)
Canidae	Caryophyllaceae (pink family)
Pristinailurus bristoli gen. et sp. nov.	
Arctomeles dimolodontus sp. nov.	

Excluding fishes and amphibians.